Layer Priors And Encoding-decoding Network For Image Dehazing

Chu Zhao[1], Hang Li[1*], and Man Jiang[2*]

[1] College of Artificial Intelligence, Shenyang Normal University, Shenyang 110034 China
[2] Liaoning Vocational Technical College of Modern Service, Shenyang, 110164, China
[*] Corresponding author. E-mail: lihangsoft@163.com and hsiaoweiw@163.com

Received: June 03, 2025; Accepted: October 01, 2025

In order to solve the shortcomings of the current image dehazing algorithm, which has poor recovery effect and general timeliness, a novel image dehazing algorithm combining the layer priors and encoding-decoding network is proposed. Firstly, the haze image is divided into background layer and haze layer, and the time gradient of background layer and horizontal gradient of haze layer and the pre-trained Gaussian mixture model corresponding to each layer are used as the prior conditions to construct the model function. Then, a channel attention module is added at the end of the encoder and the beginning of the decoder to assign different weights to the haze related feature maps extracted by the encoder and calculate the transmittance accurately. Thirdly, using the proposed fuzzy partition entropy graph cutting algorithm, the transmittance is divided into close-range, mid-range and far-range under different scene light coverage. The experimental results show that the new algorithm has a good dehazing effect on both synthetic and real fog maps compared with other dehazing methods.

Keywords: Image dehazing; Gaussian mixture model; Layer priors; Encoding-decoding network; Fuzzy partition entropy graph cutting algorithm

http://dx.doi.org/10.6180/jase.202606_29(6).0007

1. Introduction

In a haze environment, affected by the scattering of suspended water droplets and aerosols in the atmosphere, quality degradation such as low contrast and tone shift appear in captured images, which affects the function of the outdoor visual system [1, 2]. Therefore, haze image sharpening processing is of great significance for outdoor vision system [3]. Most of the existing dehazing methods are based on the physical imaging model of atmospheric scattering, and the transmittance and atmospheric light in the model are calculated to obtain the free haze image [4, 5]. Considering the different spatial positions of different targets in the scene and the influences of ambient light are also different, Ju et al. [6] proposed the improved atmospheric scattering model (IASM) considering the light of changing scenes. Based on this improved model, the transmittance, scene light and clear image are solved in this paper.

Different from the transmittance estimation algorithm based on a priori, deep learning can learn haze related information from many haze image sample data and establish a mapping relationship between the original image and transmittance, which has good robustness. For example, DehazeNet proposed by Cai et al. [7] used neural networks to directly estimate the transmittance from haze images, and obtained atmospheric light based on the low transmittance value of distant regions, so as to obtain dehazed images. Zhang et al. [8] proposed densely connected pyramid dehazing network (DCPDN) to jointly learn the results of atmospheric light, transmittance and haze removal. However, in the process of transmission estimation, the network did not consider the difference in the processing of the feature graphs of different information, which limited the performance of the network. Therefore, the channel

attention mechanism is introduced into the transmission estimation network to make the network pay attention to the important channel feature graphs and estimate the transmission efficiently and accurately [9].

On the other hand, in order to obtain the changing scene light, the haze removal algorithm based on image segmentation is widely used. Yin et al. [10] divided the image into different regions according to the haze concentration information in the haze map, calculated the scene light according to the gray value of the incident light in each region, and calculated the transmittance according to the maximum contrast in each region. Finally, the total variational guidance model was used to eliminate the boundary effect in the transmittance map and obtain a clear image. Gao et al. [11] put forward the multi-region fusion method (MRFM), which divided the haze map into sky region and non-sky region, and used the anisotropic diffusion model to fuse and optimize the transmission values of sky region and non-sky region, so as to obtain haze removal images. Yoon et al. [12] proposed wavelength adaptive dehazing (WAD) algorithm, which correlated haze concentration with light wavelength and object color, and divided haze image into long view, medium view and near view according to the color of object in the scene, thereby obtaining the transmission rate and scene light of each region. However, in the process of image segmentation to obtain scene light, the above method does not consider the spatial correlation of the scene, and it is easy to mistakenly divide the white foreground target into the distant haze area. Therefore, this paper proposes a fuzzy partition entropy graph cutting algorithm to partition the scene optical region, and integrates the graph cutting algorithm considering spatial correlation into the fuzzy partition entropy to solve the problem of misclassification caused by similar pixel values in different regions.

This new algorithm is based on the improved atmospheric scattering imaging model considering the changing scene light, and uses the channel attention neural network to predict the transmission, and uses the fuzzy partition entropy graph cutting algorithm to divide different scene light regions to calculate the scene light and atmospheric light, and obtain the haze removal image. The new algorithm has the following advantages: 1) the time direction gradient and the horizontal direction gradient are used as the network prior; 2) A transmission estimation network of channel attention mechanism is proposed, which introduces the channel attention mechanism into the coding and decoding network to make it pay attention to important channel feature maps and improve the accuracy of transmission estimation; 3) Fully consider the spatial correlation of the scene, and use the fuzzy partition entropy graph cutting algorithm to divide the transmittance map into three regions: near, middle and distant, so as to obtain accurate atmospheric light and scene light.

2. Materials and methods

2.1. Physical imaging model of atmospheric scattering

The common atmospheric scattering physical imaging model can be expressed as Eq. (1).

$$I(x,y) = J(x,y)t(x,y) + A[1 - t(x,y)] \tag{1}$$

Where (x, y) is the coordinate position index of pixel. I is haze image. t is transmittance. J is clear image. A is atmospheric light.

It can be seen from Eq. (1) that haze images all come from atmospheric light [13]. However, in the actual imaging process, due to the occlusion of the scene and the difference in reflectivity and absorptivity of different objects, the imaging is actually jointly affected by atmospheric light and scene light, and it is not accurate to only consider atmospheric light in the imaging process. Therefore, the $I(x,y)$ can be rewritten as Eq. (2),

$$I(x,y) = R(i)\rho(x,y)t(x,y) + A[1 - t(x,y)] \tag{2}$$

Where $J(x,y)$ is expressed as $R(i)\rho(x,y)$.$R(i)$ is the scene light intensity at the i position in the image, which is affected by the location information of the scene. $\rho(x,y)$ is the pixel value of the clear image at the coordinate (x,y). Here $(x,y) \in E(i)$.$E(i)$ is the set of all pixels in scene i. $t(x,y)$ represents the transmission rate of the imaging point (x, y) in the atmosphere, and its value is affected by the atmospheric scattering coefficient and depth of field in the transmission process, and decreases in an exponential order, which can be expressed as Eq. (3).

$$t(x,y) = e^{-\beta d(x,y)} \tag{3}$$

Where $d(x,y)$ is the imaging distance of the imaging point (x,y), and β is the scattering coefficient. From equation (2), it can be seen that ρ can be obtained by accurately estimating R, A, and t.

2.2 Haze removal algorithm based on layer prior

Generally, a haze image can be regarded as the superposition of a haze-free background layer B and a haze-free layer R. The purpose of dehazing is to obtain the background layer and haze layer of the haze image through decomposition, but this is an ill-posed problem. Therefore, reference [14] proposed a joint probability method to maximize the background layer and the haze layer by using the maximum a posterior probability (MAP). After a certain

mathematical transformation, the model can be equivalent to solving the minimum value of the energy function as Eq. (4).

$$\min_{B,R} \|O - B - R\|_F^2 + \Phi(B) + \Psi(R) \tag{4}$$

Where $\|\cdot\|_F$ is the Frobenius norm. O is the haze image. The value of each pixel in the optimal solution B and R should not be greater than the corresponding value in O and not less than 0.$\Phi(B)$ and $\Psi(R)$ are the prior conditions of the background layer and the haze layer respectively, which are used to regularize the two layers and can be expressed as Eqs. (5) and (6).

$$\Phi(B) = -\gamma \sum_i \log G_B\left[P_i(B)\right] + \alpha \|\nabla B\|_1 \tag{5}$$

$$\Psi(R) = -\gamma \sum_i \log G_R\left[P_i(R)\right] + \beta \|R\|_f^2 \tag{6}$$

Where $P(\cdot)$ is the i -th block of the corresponding layer. $G(\cdot)$ is the probability density of the image block in the corresponding GMM. ∇B is the gradient of the haze layer. γ, α and β are the coefficients of the corresponding terms. The layer prior algorithm uses a pre-trained GMM model with 200 Gaussian components [15] as one of the priors of the background layer. In addition, at the beginning of the algorithm, a lightweight GMM model is trained online by using the artificially marked obvious rain area as the training image, as one of the priors of the haze layer. In order to facilitate the solution, logarithmic form and L1 norm regularization are adopted, and gradient is also a prior knowledge commonly used in the field of image restoration in recent years [16, 17].

2.2. Transmission estimation network based on encoder-decoder network

The network structure of transmittance estimation based on encoder-decoder is shown in Fig. 1, including shallow feature extraction, encoder, decoder and mapping layer.

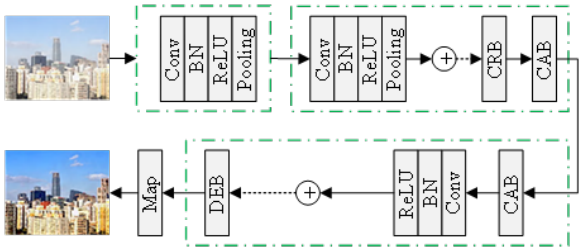

Fig. 1. Transmission estimation network based on encoder-decoder network.

1. Shallow feature extraction. Extraction of shallow feature maps, such as edge, texture and contour, is conducive to the mining of deep feature maps. A shallow feature extraction module is constructed using Convolution (Conv), Normalization (BN), Rectified Linear Unit (ReLU) [18] and pooling layers with a size of 3×3 and step size of 1.

$$F_S = H_{SF}(I) \tag{7}$$

Where I is the input haze map. H_{SF} is a function of shallow feature extraction operator. F_S is the output of the H_{SF} and also the input to the encoder.

2. Encoder. The convolutional residual block (CRB) and channel attention block (CAB) are used for construction. CRB introduces residual connection on the basis of shallow feature extraction module (Fig. 1). In addition, CAB is added at the end of the encoder to assign different channel feature map weights to the feature maps extracted by CRB, so that the network pays more attention to important information related to the transmission estimation task, such as dense fog information. Therefore, the encoder function can be defined as Eq. (8).

$$\begin{aligned} &F_d = H_{EN}\left(F_s\right) = \\ &H_{CAB}\left\{H_{CRB,d}\left\{\cdots\left[H_{CRB,1}\left(F_s\right)\right]\cdots\right\}\right\} \end{aligned} \tag{8}$$

Where $H_{EN}(\cdot)$ represents the encoder function. $H_{CRB,d}$ represents the $d-th$ convolutional residual module function. H_{CAB} represents the channel attention module function. F_d is the output of the encoder.

3. Decoder. To reconstruct the transmittance, the F_d is symmetrically upsampled using a deconvolution block (DEB). The first step of the decoder still uses CAB to assign the appropriate weight to F_d, and then uses a combination of deconvolution (Deconv), batch normalization (BN) and rectified linear unit (ReLU) and the DEB module of residual connection implement upsampling operation step by step.

$$\begin{aligned} &F_b = H_{DE}\left(F_d\right) = \\ &H_{DEB,b}\left\{\cdots H_{DEB,2}\left\{\left\{H_{DEB,1}\left[H_{CAB}\left(F_d\right)\right]\right\}\right\}\right\} \end{aligned} \tag{9}$$

Where F_b is the output of the decoder. $H_{DE}(\cdot)$ is the decoder function. $H_{DEB,b}$ stands for the $b-$ th deconvolution module function.

4. Mapping layer. At the end of the network, a convolution layer is used to map the feature map to the transmittance map, and the function of the mapping layer can be expressed as Eq. (10).

$$t = H_{MAP}\left(F_b\right) \tag{10}$$

Where $H_{\mathrm{MAP}}(\cdot)$ is the mapping layer function. t is the output of the mapping layer and also the transmittance map estimated by the network. The transmittance estimation network based on channel attention uses the loss function L to search the optimal parameters of the model.

$$L = L_2 + \lambda L_g + \beta L_f \tag{11}$$

In the formula, λ and β are the weight coefficient of L_g, and L_f respectively. The expression of L_2 is as Eq. (12).

$$L_2 = \frac{1}{N}\sum_{i=1}^{N}\left\|H_{CAN}\left(I^i\right) - t^2\right\|_2 \tag{12}$$

Where $\left\{I^i, t^i\right\}_{i=1}^{N}$ represents N haze images and the corresponding true transmittance. H_{CAN} represents the function of the channel attention network, and $H_{CAN}\left(I^i\right)$ is the estimated transmission of the channel attention network when the $i-$ th haze image is input. The expression for L_g is shown in Eq. (13).

$$\begin{aligned} L_g = \frac{1}{N}\Bigg\{&\sum_{i=1}^{N}\left\|G_v\left[H_{CAN}\left(I^i\right)\right]\right. \\ &\left.-G_v\left(t^i\right)\right\|_2 + \sum_{i=1}^{N}\left\|G_h\left[H_{CAN}\left(I^i\right)\right] - G_h\left(t^i\right)\right\|_2\Bigg\} \end{aligned} \tag{13}$$

Where G_v and G_h are operators for calculating the vertical and horizontal gradients of the image respectively.

$$\begin{aligned} L_f = \frac{1}{N}\Bigg\{&\sum_{i=1}^{N}\left\|F_{v1}\left[H_{CAN}\left(I^i\right)\right]\right. \\ &\left.-F_{v1}\left(t^i\right)\right\|_2 + \sum_{i=1}^{N}\left\|F_{v2}\left[H_{CAN}\left(I^i\right)\right] - F_{v2}\left(t^i\right)\right\|_2\Bigg\} \end{aligned} \tag{14}$$

2.3. Scene light estimation and image de-hazing

The scene light factor of different regions is estimated from the corresponding scene region E, so it is particularly important to accurately divide the scene light region. The transmission rate is divided into near, middle and long range by using the fuzzy partition entropy graph cutting algorithm. This method incorporates the graph cutting algorithm considering spatial correlation into the threshold segmentation algorithm, which not only avoids regional misclassification, but also facilitates accurate estimation of scene light and atmospheric light.

The fuzzy 3-partition entropy algorithm [19] is used to search the optimal threshold for dividing the pixel sets of near scene E_b, middle scene E_m and long scene E_d. Membership functions M_d, M_m, M_b for sets E_d, E_m, E_b are defined using the S function and its inverse function $Z = 1 - S$. Then the fuzzy partition probability of each set is as Eq. (15).

$$P_b = \sum_{k=1}^{255} h(k)M_b, P_m = \sum_{k=1}^{255} h(k)M_m, P_d = \sum_{k=1}^{255} h(k)M_d \tag{15}$$

Where $h(\cdot)$ is the transmittance histogram, and the probability of occurrence of any grayscale k in the transmittance is calculated. P_b, P_m, P_d divide the probabilities for the set of E_b, E_m, and E_d.

The fuzzy 3-partition entropy model of the transmittance graph is shown in Eq. (16). The iterative strategy-based method [20] can be used to quickly search the threshold of dividing E_d, E_m, E_b sets when the fuzzy entropy is maximum.

$$H = -P_d\log(P_d) - P_m\log(P_m) - P_b\log(P_b) \tag{16}$$

The threshold determined by the maximum fuzzy entropy is directly used to divide the pixels, without considering the spatial correlation of pixels, which is easy to cause regional misclassification due to the similar transmission values of different regions. Therefore, the graph cutting algorithm [21] considering spatial correlation is integrated into the fuzzy partition entropy, and the fuzzy partition entropy graph cutting algorithm is proposed. The energy function E of graph cutting is expressed as Eq. (17).

$$E = \lambda D\left(l_p\right) + Q\left(l_p, l_q\right) \tag{17}$$

Where p and q are adjacent pixels. l_p and l_q are labels, and their values can be long view "d", middle view "m" and near view "b". $D\left(l_p\right)$ is the data item, representing the cost of pixels in the transmittance being divided into label l_p.$Q\left(l_p, l_q\right)$ is the smooth term, representing the cost of p and q marked as l_p and $l_q \cdot \lambda = 1$ is the balance factor between the data item and the smooth item. For $D\left(l_p\right)$, the set partition probability at the maximum of Eq. (16) is used to design.

$$\begin{cases} D\left(l_p = "b"\right) = -\log\left(P_b\right) \\ D\left(l_p = "m"\right) = -\log\left(P_m\right) \\ D\left(l_p = "d"\right) = -\log\left(P_d\right) \end{cases} \tag{18}$$

The smooth term is defined as Eq. (19),

$$Q\left(l_p, l_q\right) = \exp\left(-\frac{\left(k_p - k_q\right)^2}{2\delta^2}\right) \times \frac{1}{\mathrm{dist}(p,q)} \tag{19}$$

Where, k_p and k_q are the gray levels of adjacent pixels p and q.δ is the variance between adjacent pixels. dist (p,q) is the Euclidean distance between pixels p and q. After the graph cut model is constructed, $\alpha - \beta$ exchange algorithm

is used to solve the graph cut model, so as to obtain the optimal partition of E_d, E_m, E_b sets.

From the divided pixels set of E_d, E_m, E_b, the top 1% pixels with the highest brightness value in the initial haze map are selected, and their brightness mean value is taken as the scene light of each collection area, and the initially estimated scene light R is obtained. However, the scene light R estimated by the above method has obvious boundary effect, which is inconsistent with the real situation. In order to approximate the real result, the regular optimization algorithm is used to refine the scene light.

$$R' = \operatorname{argmin}\left\{\left\|R - R'\right\|_2^2 + \theta_1 \left\|\nabla\left(R'\right) - \nabla(G)\right\|_2^2\right\} \quad (20)$$

Where $\theta_1 = 0.4$ is the regularization parameter. G is the brightness component of the haze image. ∇ is the gradient operator. The first term of Eq. (20) ensures that the optimized scene light R' approximates the segmentation result of the fuzzy partition entropy graph cut, while the second term constrains the edge features of R' so that it is consistent with G. The optimized scene light R' can be obtained by adopting the iterative optimization strategy.

Given the atmospheric light intensity A, scene light R', and transmittance t, a clear image ρ can be obtained by Eq. (2). In order to avoid the denominator being infinite because t is too small, the lower limit of t is set t_0, and a clear image can be calculated by Eq. (21).

$$\rho = \frac{I - A\left[1 - \max\left(t, t_0\right)\right]}{R' \max\left(t, t_0\right)} \quad (21)$$

3. Results and discussion

3.1. Experiment Settings

A PC is used for model training and testing. The CPU is Intel Core i9-7900X, the main frequency is 3.30GHz, the memory is 64 GB, and the GPU is a NVIDIA RTX 3080Ti graphics card. All experiments in this paper are designed and implemented under the Pytorch deep learning framework. In the training process, the training image is randomly cropped to 256×256 pixels, the batch size is set to 4, and the training is 50 rounds. In addition, the Adam optimizer with the attenuation coefficient as the default is used to speed up the training process, the initial learning rate is set to 0.001, and it is reduced by half every 5 turns.

The algorithm is trained on ITS, and tested on both synthetic and real haze image datasets. The training set contains 1399 clean images and 13990 paired haze images. In order to verify the effectiveness and superiority of the proposed algorithm, DCP [22], NLD [23], DA [24], EPDN [25] and PSD [26] de-hazing algorithms are selected for experimental testing and comparison.

3.2. Experimental results on synthetic haze images

Qualitative comparison is made on the test set SOTS in RESIDE dataset, and the experimental results are shown in Fig. 2. As can be seen from Fig. 2, the DCP method based

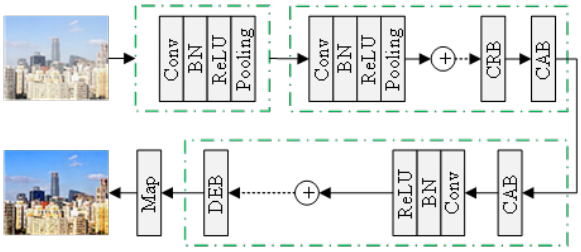

Fig. 2. Comparison of different methods on the SOTS test set.

on prior information can effectively de-haze the image, but the generated de-haze image will produce serious color distortion. As shown in Fig. 2, the sky region of the DCP method is abnormally blue. In addition, compared with the clear image, the brightness of the haze removal image generated by DCP is darker, which seriously affects the visual perception effect of people. Similar to the DCP, the NLD also fails to effectively remove the haze in the sky region of the image because the prior information of unilateral assumption is not applicable to all scenes, and the de-hazing image generated by the NLD algorithm produces unnecessary artifacts. The de-hazing image generated by DA algorithm has a satisfactory visual effect, but it still causes a certain degree of color distortion in some images. EPDN can effectively remove haze in the image, but it will make the brightness of the generated image dim and the contrast decrease. The image generated by PSD algorithm has high brightness and contrast, but the color susaturation also makes the image generated by this PSD algorithm look unreal. Compared with other algorithms, the haze removal image generated by the proposed algorithm LPEDN is more natural in color, clearer in texture and higher in fidelity.

To further verify the performance of LPEDN, we conduct quantitative comparison on RESIDE dataset. The evaluation indexes are Peak Signal-to-Noise Ratio (PSNR) and SSIM. The experimental results are shown in Table 1.

As can be seen from Table 1, on the indoor data set, the proposed algorithm obtains the optimal image haze removal results, whose PSNR and SSIM are 30.98dB and 0.983, respectively. On outdoor data sets, the proposed algorithm also achieves the best de-hazing results, and compared with the second-best algorithm DA, the proposed algorithm increases PSNR from 22.70dB to 23.68dB, and SSIM from 0.928 to 0.935. The above experimental results

Fig. 3. Comparison of different methods on the URHI test set.

Table 1. Quantitative experimental results of different methods on SOTS dataset.

Method	Indoor data set		Outdoor data set	
	PSNR/dB	SSIM	PSNR/dB	SSIM
DCP	20.06	0.873	20.55	0.899
NLD	17.40	0.802	18.22	0.872
EPDN	25.20	0.933	20.43	0.903
PSD	16.43	0.730	15.26	0.772
DA	30.43	0.982	22.70	0.928
LPEDN	30.98	0.983	23.68	0.935

show that LPEDN can effectively remove haze on both indoor and outdoor data sets.

3.3. Experimental results on real haze image

In order to further verify the performance of LPEDN, it is compared with other algorithms on the real haze data set URHI. Experimental results are shown in Fig. 3.

As can be seen from Fig. 3, DCP tends to dim the brightness of the image after haze removal, especially in the sky area, which will produce artifacts, thus affecting the visual effect of the haze removal image. Although the NLD algorithm can effectively de-haze the image, the generated de-haze image has serious color distortion, which makes its visual effect poor. In contrast, image de-hazing methods based on deep learning often result in less thorough de-hazing, resulting in under-hazed images. For example, DA and EPDN will still cause a certain degree of haze residue in some areas of the image, and the texture features of the image are not obvious. The image generated by PSD is brighter and has higher contrast. However, due to the excessive enhancement in some areas, the image generated by PSD is still over-saturated to a certain extent [27, 28]. In contrast, the LPEDN algorithm enables the model to effectively de-haze while avoiding the color distortion of de-hazing image generated in the de-hazing process to a great extent, thus presenting a better de-hazing effect on the real image with haze. Also, the detailed results are shown in Table 2. It can also be concluded that the new algorithm in this paper obtains the optimal result.

Table 2. Quantitative experimental results of different methods on URHI dataset.

Method	PSNR/dB	SSIM
DCP	18.51	0.814
NLD	19.77	0.827
EPDN	20.59	0.862
PSD	21.65	0.887
DA	23.81	0.939
LPEDN	24.97	0.946

3.4. Running time comparison

The running time of this algorithm consists of the transmission estimation time of channel attention network and the calculation time of scene light and atmospheric light. The encoder and decoder of the network each contain four modules, the network layer number is small, the framework is simple, and the transmittance of a single haze image is estimated to be only 0.2 s . On the other hand, when estimating atmospheric light and scene light, the recursive strategy is used to search for maximum fuzzy entropy. The average running time of a single image is 0.2 s , and the subsequent $\alpha - \beta$ exchange algorithm takes only 3 s to solve the graph cut model. Finally, it takes 0.5 s to solve the canonical optimization model by gradient descent method. As shown in Table 3, the running time of the proposed algorithm is 3.9s

in total, which is better than that of DA algorithm and PSD algorithm. Although the running time is longer than that of EPDN algorithm and NLD algorithm, it can be seen from Tables 1 and 2 that the de-hazing effect of the proposed algorithm is obviously better than that of PSD algorithm and DA algorithm.

Table 3. Running time comparison with different methods.

Method	NLD	EPDN	PSD	DA	LPEDN
Time/s	2.5	1.79	4.4	4.6	3.9

4. Conclusions

This paper presents a haze removal algorithm based on layer prior and encoder-decoder network. When using the encoder-decoder network to estimate transmission, a channel attention module is added in the middle of the encoder and decoder to assign different weights to the feature maps containing different information, so that the network is more sensitive to important feature maps (such as the feature map containing haze information) and provide more effective information for the subsequent network layer. In the estimation of scene light and atmospheric light, the transmission is divided into near, middle and distant by using the fuzzy entropy graph cutting algorithm, and the corresponding scene light and atmospheric light are extracted from each region. In this strategy, the graph cut algorithm considering spatial correlation is integrated into the fuzzy partition entropy algorithm to ensure that the regions with similar transmission values will not be misclassified. The experimental results show that both objective and subjective results are superior to the existing de-hazing algorithms. It can be seen that accurate prediction of transmission and full consideration of changing scene light can improve the accuracy of image haze removal. However, the new algorithm uses fuzzy partition entropy graph cut and scene light iterative optimization algorithm to estimate the changing scene light, which reduces the efficiency of de-hazing, and the average de-hazing time of a single image is 3.9s. In the future, the process of solving scene light will be further optimized to improve efficiency, so that it can be applied to engineering practice such as intelligent driving.

Acknowledgment

This work was supported by the "Research on the Application of Knowledge Base-driven Enhanced Large Language Models in the Scenario of Education and Teaching: Construction of a Platform Project-Key Cultivation Project", project number: LJ232410166062.

References

[1] G. Dimas, D. E. Diamantis, P. Kalozoumis, and D. K. Iakovidis, (2020) *"Uncertainty-aware visual perception system for outdoor navigation of the visually challenged"* **Sensors *20***(8): 2385. DOI: 10.3390/s20082385.

[2] E. Zambrano-Serrano, S. Bekiros, M. A. Platas-Garza, C. Posadas-Castillo, P. Agarwal, H. Jahanshahi, and A. A. Aly, (2021) *"On chaos and projective synchronization of a fractional difference map with no equilibria using a fuzzy-based state feedback control"* **Physica A: Statistical Mechanics and its Applications *578***: 126100. DOI: 10.1016/j.physa.2021.126100.

[3] M. Bataineh, M. Alaroud, S. Al-Omari, and P. Agarwal, (2021) *"Series representations for uncertain fractional IVPs in the fuzzy conformable fractional sense"* **Entropy *23***(12): 1646. DOI: 10.3390/e23121646.

[4] L. Teng, Y. Qiao, and S. Yin, (2024) *"Underwater image denoising based on curved wave filtering and two-dimensional variational mode decomposition"* **Computer Science and Information Systems *21***(4): 1765–1781. DOI: 10.2298/CSIS240314057T.

[5] T. Rasham, M. S. Shabbir, P. Agarwal, and S. Momani, (2022) *"On a pair of fuzzy dominated mappings on closed ball in the multiplicative metric space with applications"* **Fuzzy sets and systems *437***: 81–96. DOI: 10.1016/j.fss.2021.09.002.

[6] M. Ju, D. Zhang, and X. Wang, (2017) *"Single image dehazing via an improved atmospheric scattering model"* **The Visual Computer *33***(12): 1613–1625. DOI: 10.1007/s00371-016-1305-1.

[7] B. Cai, X. Xu, K. Jia, C. Qing, and D. Tao, (2016) *"Dehazenet: An end-to-end system for single image haze removal"* **IEEE transactions on image processing *25***(11): 5187–5198. DOI: 10.1109/TIP.2016.2598681.

[8] H. Zhang and V. M. Patel. "Densely connected pyramid dehazing network". In: *Proceedings of the IEEE conference on computer vision and pattern recognition*. 2018, 3194–3203. DOI: 10.1109/CVPR.2018.00337.

[9] S. Yin, L. Wang, and L. Teng, (2024) *"Threshold segmentation based on information fusion for object shadow detection in remote sensing images"* **Computer Science and Information Systems *21***(4): 1221–1241. DOI: 10.2298/CSIS231230023Y.

[10] L. Yin, L. Wang, W. Huang, S. Liu, B. Yang, and W. Zheng, (2021) *"Spatiotemporal analysis of haze in Beijing based on the multi-convolution model"* **Atmosphere *12***(11): 1408. DOI: 10.3390/atmos12111408.

[11] Y. Gao, Q. Li, and J. Li, (2020) *"Single image dehazing via a dual-fusion method"* **Image and Vision Computing *94***: 103868. DOI: 10.1016/j.imavis.2019.103868.

[12] I. Yoon, S. Jeong, J. Jeong, D. Seo, and J. Paik, (2015) *"Wavelength-adaptive dehazing using histogram merging-based classification for UAV images"* **Sensors *15***(3): 6633–6651. DOI: 10.3390/s150306633.

[13] S. An, X. Huang, L. Cao, and L. Wang, (2024) *"A comprehensive survey on image dehazing for different atmospheric scattering models"* **Multimedia Tools and Applications *83***(14): 40963–40993. DOI: 10.1007/s11042-023-17292-8.

[14] Y. Wang, F. Fu, F. Lai, W. Xu, J. Shi, and J. Wang, (2019) *"Haze removal algorithm based on single-images with chromatic properties"* **Signal Processing: Image Communication *72***: 80–91. DOI: 10.1016/j.image.2018.12.010.

[15] H. Fu, W. Liu, H. Chen, and Z. Wang, (2020) *"An anisotropic Gaussian filtering model for image de-hazing"* **Ieee Access *8***: 175140–175149. DOI: 10.1109/ACCESS.2020.3026185.

[16] M. Shams, N. Kausar, P. Agarwal, and S. Jain. "Fuzzy fractional Caputo-type numerical scheme for solving fuzzy nonlinear equations". In: *Fractional Differential Equations*. Elsevier, 2024, 167–175. DOI: 10.1016/B978-0-44-315423-2.00016-3.

[17] L. Shafi, S. Jain, P. Agarwal, P. Iqbal, and A. R. Sheergojri, (2024) *"An improved fuzzy time series forecasting model based on hesitant fuzzy sets"* **Journal of fuzzy extension and applications *5***(2): 173–189. DOI: 10.22105/jfea.2024.432442.1357.

[18] S. Yin, H. Li, A. A. Laghari, T. R. Gadekallu, G. A. Sampedro, and A. Almadhor, (2024) *"An anomaly detection model based on deep auto-encoder and capsule graph convolution via sparrow search algorithm in 6G Internet of Everything"* **IEEE Internet of Things Journal *11***(18): 29402–29411. DOI: 10.1109/JIOT.2024.3353337.

[19] A. R. Abbasi, (2020) *"Probabilistic load flow based on holomorphic embedding, kernel density estimator and saddle point approximation including correlated uncertainty variables"* **Electric Power Systems Research *183***: 106178. DOI: 10.1016/j.epsr.2019.106178.

[20] A. R. Abbasi and A. R. Seifi, (2013) *"A new coordinated approach to state estimation in integrated power systems"* **International Journal of Electrical Power & Energy Systems *45***(1): 152–158. DOI: 10.1016/j.ijepes.2012.08.058.

[21] D. Adla, G. Reddy, P. Nayak, and G. Karuna, (2023) *"A full-resolution convolutional network with a dynamic graph cut algorithm for skin cancer classification and detection"* **Healthcare Analytics *3***: DOI: 10.1016/j.health.2023.100154.

[22] B. S. Krishna, A. S. Anandhi, G. Sharmila, D. Ramya, L. Balaji, and B. Pasupulati. "A Method for Image De-Hazing for Vision Based Applications". In: *2024 International Conference on Computational Intelligence for Green and Sustainable Technologies (ICCIGST)*. IEEE. 2024, 1–6. DOI: 10.1109/ICCIGST60741.2024.10717509.

[23] J. S. Bhadoria and D. Agarwal. "Enhanced Image De-Hazing Using Novel Hybrid Filtering and Perceptual Fog Density Improvement". In: *2023 International Conference on Computing, Communication, and Intelligent Systems (ICCCIS)*. IEEE. 2023, 562–567. DOI: 10.1109/ICCCIS60361.2023.10425763.

[24] J. A. H. Shaikh, S. M. Mukane, and S. N. Randive, (2025) *"Lightweight progressive recurrent network for video de-hazing in adverse weather conditions"* **The Visual Computer *41***(7): 4661–4672. DOI: 10.1007/s00371-024-03683-x.

[25] E. Radha, D. Suresha, and E. Ramesh. "Design and Implementation of Image De-hazing Using Histogram Equalization". In: *Mobile Radio Communications and 5G Networks: Proceedings of Third MRCN 2022*. Springer, 2023, 343–351. DOI: 10.1007/978-981-19-7982-8_28.

[26] M. T. Ahmed, S. H. Bappy, J. K. Tuly, and T. Billah, (2023) *"An Effective Single Image Dehazing Method to Enhance Image Visibility"* **Journal of Information Technology *12***(1): 1–12. DOI: 10.6035/14028.2017.178642.

[27] A.-R. Abbasi, R. Khoramini, B. Dehghan, M. Abbasi, and E. Karimi, (2015) *"A new intelligent method for optimal allocation of D-STATCOM with uncertainty"* **Journal of Intelligent & Fuzzy Systems *29***(5): 1881–1888. DOI: 10.3233/ifs-151666.

[28] A. Kavousi-Fard, R. Khorram-Nia, M. Rostami, and A. Abbasi, (2015) *"An smart stochastic approach to model plug-in hybrid electric vehicles charging effect in the optimal operation of micro-grids"* **Journal of Intelligent & Fuzzy Systems *28***(2): 835–842. DOI: 10.3233/ifs-141365.